



Enabling High Lithium Conductivity in Polymerized Ionic Liquid Block Copolymer Electrolytes

Nicolas Goujon,^{*[a]} Tan-Vu Huynh,^[a] Kristine j. Barlow,^[a, b] Robert Kerr,^[a] Keti Vezzù,^[c] Vito Di Noto,^[c] Luke A. O'Dell,^[a] John Chiefari,^[b] Patrick C. Howlett,^[a] and Maria Forsyth^[a]

Herein, the use of a novel block copolymer host, based on a polymerized ionic liquid block copolymer, is proposed. Mechanically robust solid polymer electrolytes (SPEs) with high lithium conductivity are developed using a ternary polymer electrolyte system, consisting of a poly(styrene-*b*-1-((2-acryloyloxy)ethyl)-3-butylimidazolium bis(trifluoromethanesulfo-nyl)imide) (S-PIL₆₄₋₁₆) block copolymer, a *N*-propyl-*N*-methylpyrrolidinium bis(fluorosulfonyl)imide (C₃mpyrFSI) ionic liquid (IL) and a lithium bis(fluorosulfonyl) imide (LiFSI) salt. The impact of both IL and lithium salt concentration on the morphology, ion migration processes and electrochemical performance of the electrolytes is characterized. High lithium ion conductivity is achieved when anion to Li⁺ molar ratio was kept below a value of 1.5, resulting in a lithium transport number (t^{Li^+}) as high as 0.53 at 50 °C. Finally, the cycling performance in a Li|LiFePO₄ full cell is assessed using an in-house formulated solid-state high loading cathode (LiFePO₄ loading = 10 mg cm⁻², 1.8 mAh cm⁻²). 98% of the theoretical discharge capacity (167 mA g⁻¹) is achieved for the first cycle at a C-rate of C/20 at 50 °C. The results herein reported are the first demonstration of a PIL block copolymer-IL-salt composite electrolyte operating at near-practical levels, making them a promising choice of electrolyte for the next generation of solid-state high capacity lithium-metal batteries.

Lithium-ion batteries have emerged as the technology of choice that is able to satisfy a broad range of commercial applications, from small handheld electronics to electric vehicles and stationary energy storage. However, their market uptake and implementation has been significantly hampered by the low theoretical gravimetric energy density of current lithium-ion battery technologies (350–400 Wh kg⁻¹).^[1–3] Many efforts have thus been made towards the development of new

materials for the next generation of lithium-ion high energy-density electrodes^[3–5] and compatible electrolytes.^[6,7] The most intensively studied high energy-density cathodes are based on oxygen- (air) and sulphur- (S₈) chemistries.^[3,4] To fully unlock their potential in terms of a realized cell performance, these cathodes need to be used in conjunction with a high energy-density anode such as lithium-metal or silicon as the current graphite anode technology cannot match the high areal electrode capacities associated with these high capacity electrode materials (e.g. 372 mAh g⁻¹ vs. 1672 mAh g⁻¹ for graphite anode and sulphur cathode, respectively).^[3,8] When coupled with a lithium-metal anode, Li-sulphur and Li-oxygen batteries offer drastically improved theoretical energy-densities of 2613 Wh kg⁻¹ and 3458 Wh kg⁻¹, respectively.^[3]

However, the use of a lithium-metal anode in conjunction with traditional liquid-based electrolytes presents a new set of challenges: i) poor cyclability due to the formation of a passive layer at the lithium-electrolyte interface, (i.e. formation of lithium dendrites caused by irregular lithium deposition during the charging process, which in turn leads to a significantly shortened cycle life), ii) using a heavy battery case to avoid electrolyte leakage; and iii) a potential explosion hazard due to the flammable nature and volatility of traditional liquid electrolytes.^[5,9] A promising solution to overcome these challenges lies in the use of solid polymer electrolytes (SPEs) with a sufficiently high modulus.^[10,11] Indeed, Monroe *et al.* showed through computational simulations that dendritic growth could be suppressed if the shear modulus of the SPE is twice that of lithium.^[10] Shortly after, Balsara *et al.* experimentally showed that the resistance to dendritic growth was greater in the case of block copolymer electrolytes than that of its corresponding homopolymer electrolyte.^[11] This finding supports, to some extent, the hypothesis of Monroe *et al.* that an SPE with high modulus is beneficial for dendrite suppression. Designing SPEs which simultaneously possess a) a sufficiently high modulus for dendrite suppression; b) a good chemical and electrochemical stability where faced with lithium-metal anode; and c) the required ionic conductivity for satisfactory cell performance remains an elusive target due to the inverse relationship that exists between these two materials properties.^[1,7] Various strategies have been implemented in an attempt to enhance the ion conduction and/or mechanical properties of SPEs.^[12] Such approaches include; i) the incorporation of nano-fillers for mechanical reinforcement, ii) the development of innovative hybrid materials, iii) the use of plasticizers such as ionic liquids (IL) to enhance ion conduction, or iv) a combination thereof.^[13–20] However, these approaches introduce additional and

[a] Dr. N. Goujon, Dr. T.-V. Huynh, Dr. K. j. Barlow, Dr. R. Kerr, Dr. L. A. O'Dell, Prof. P. C. Howlett, Prof. M. Forsyth
Institute for Frontier Materials
Deakin University

Burwood, Victoria 3125, Australia
E-mail: nicolas.goujon@deakin.edu.au

[b] Dr. K. j. Barlow, Dr. J. Chiefari
CSIRO Manufacturing
Bag 10, Clayton, Victoria 3169, Australia

[c] Dr. K. Vezzù, Prof. V. Di Noto
Section of "Chemistry for the Technology" (ChemTec), Department of Industrial Engineering
University of Padova
Via Marzolo 9, I-35131 Padova (PD), Italy

 Supporting information for this article is available on the WWW under <https://doi.org/10.1002/batt.201800104>

often complex fabrication steps to ensure the homogeneous distribution of the additive within the membrane.^[21] While these approaches may lead to promising results at small scale, where solvent casting methods and ultrasonic mixing of the casting solution have been routinely employed to avoid particle agglomeration, there are challenges in upscaling to commercial quantities where these processes are either impractical or costly.^[21,22]

An innovative route to improving the mechanical properties of a given SPE without the introduction of nano-fillers resides in the incorporation of a block copolymer into the polymer structure, whereby a mechanically robust block is covalently bonded to the ion-conducting block. The microphase separation that is present in these materials allows the mechanical and ion-conduction properties of the SPE to be tuned independently.^[1,23–26] Polystyrene or poly(methyl methacrylate) blocks are commonly used for mechanical reinforcement or as dielectric materials, while ethylene oxide-based blocks (PEO) are most frequently used as the ion-conducting block.^[1,23–26] However, the transport properties of the lithium ion in ethylene oxide-based polymers is dictated by the segmental motions (α relaxations) of the ethylene oxide chains in the amorphous phase, which corresponds to the diffusion of conformational state along the polymer backbone chains,^[27] resulting in limited ionic conductivity at temperatures below the melting point of PEO (65 °C).^[1,28–31] Additionally, lithium ions are coordinated strongly with the coordination sites by oxygen ligands of the ethylene oxide repeat units, thereby hindering lithium ion inter-chain migration processes,^[32,33] thus resulting in a relatively small fraction of charge being carried by the lithium ion (lithium transport number, $t^{Li^+} = 0.1–0.2$).^[34–38] Such a small lithium transport number will lead to a strong concentration polarization across the cell during cycling, the result of which is the activation of side reactions with lithium dendrite formation.^[1] The development of alternative ion conducting blocks has attracted a great deal of interest over the past few decades.^[7,39] Recently, a new family of polyelectrolytes obtained by polymerizing ionic liquids (PILs), have been studied for application in lithium battery electrolytes.^[16,40–43] The repeat units of these polymers are similar in structure to the present ionic liquids (ILs), PILs offer the potential to exhibit a unique set of desirable properties such as high ionic conductivity, good chemical, electrochemical and thermal stability, coupled with the intrinsic advantages of polymeric polyelectrolyte materials, which include ease of processing and no leakage.^[41–43] However, PIL-based electrolyte membranes, as with any homopolymer host, suffer from a rapid deterioration of the mechanical properties when doped with either an IL and/or a lithium salt due to plasticizing effects.^[16,17,40]

Herein, the development of a ternary polymer electrolyte system is described using a novel PIL block copolymer, where a polystyrene block is used for mechanical reinforcement. This ternary polymer electrolytes system consists of a poly(styrene-*b*-1-((2-acryloyloxy)ethyl)-3-butylimidazolium bis(trifluoromethanesulfonfyl)imide) block copolymer, denoted as S-PIL₆₄₋₁₆, a *N*-propyl-*N*-methylpyrrolidinium bis(fluorosulfonyl)imide (C₃mpyrFSI) ionic liquid (IL) and a lithium bis (fluorosulfonyl) imide

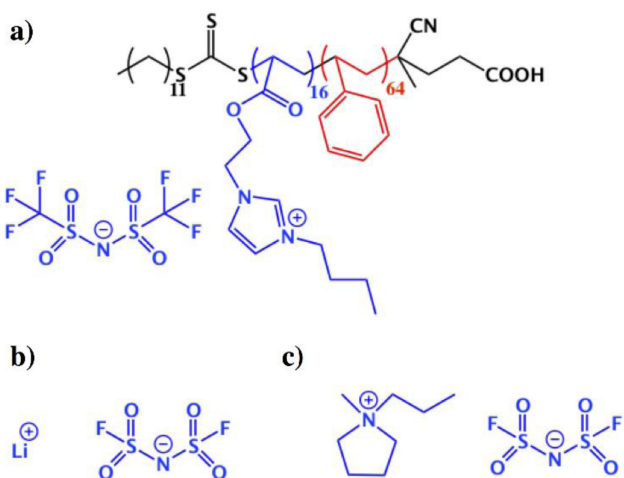


Figure 1. Chemical structure of the S-PIL₆₄₋₁₆ (a), LiFSI (b) and C₃mpyrFSI (c).

(LiFSI) salt and their chemical structure is presented in Figure 1. The number of styrene and PIL repeat units used in this work is 64 and 16, respectively.

As suggested by the differential scanning calorimetry (DSC) and small-angle X-ray scattering (SAXS) results, the pristine S-PIL₆₄₋₁₆ polymer shows strong signs of microphase separation, in which the PIL and polystyrene (PS) phases are organized in a lamellar fashion (See Figure S1 and S2). The addition of either IL or LiFSI results in a decrease in the glass transition temperature (T_g) of the PIL phase (T_g -PIL) while T_g of the PS phase (T_g -PS) remains unaffected, suggesting a selective solubility and a plasticizing behaviour towards the PIL phase.^[13,44] The addition of IL into the pristine S-PIL₆₄₋₁₆ (Li: 0.00; IL: 0.39) has little to no effect on the lamellar morphology. On the other hand, the addition of LiFSI results in a significant broadening of the diffraction peaks observed, suggesting the formation of a less ordered lamellar morphology with a broader D-spacing distribution. See Supporting Information for a more details discussion of the DSC and SAXS results.

Electrochemical impedance spectroscopy (EIS) and lithium pulsed field gradient (PFG) diffusion NMR were performed to investigate the impact of IL and LiFSI addition on the ion dynamics of the S-PIL₆₄₋₁₆ electrolytes. Figure 2a shows the ionic conductivity as a function of temperature for the pristine S-PIL₆₄₋₁₆ as well as the S-PIL₆₄₋₁₆ electrolytes. The addition of IL to pristine S-PIL₆₄₋₁₆ (Li: 0.00; IL: 0.39) results in a significant increase in ionic conductivity, which is consistent with the decrease in T_g -PIL observed from the DSC data in Figure S1. The pristine S-PIL₆₄₋₁₆ and the S-PIL₆₄₋₁₆ (Li: 0.00; IL: 0.39) system exhibit an ionic conductivity of 1.7×10^{-7} Scm⁻¹ and 4.0×10^{-6} Scm⁻¹ at 50 °C, respectively. As LiFSI is first introduced into the S-PIL₆₄₋₁₆ (Li: 0.58; IL: 0.39), a slight increase in ionic conductivity is observed, resulting in an ionic conductivity of 7.6×10^{-6} Scm⁻¹ at 50 °C. We believe this increase in ionic conductivity is due to an increase in the overall ion concentration in the polymer system. A further increase in Li molar ratio results in a slight decrease in the ionic conductivity to 6.6×10^{-6} Scm⁻¹ at 50 °C for S-PIL₆₄₋₁₆ (Li: 5.81; IL: 0.39). The

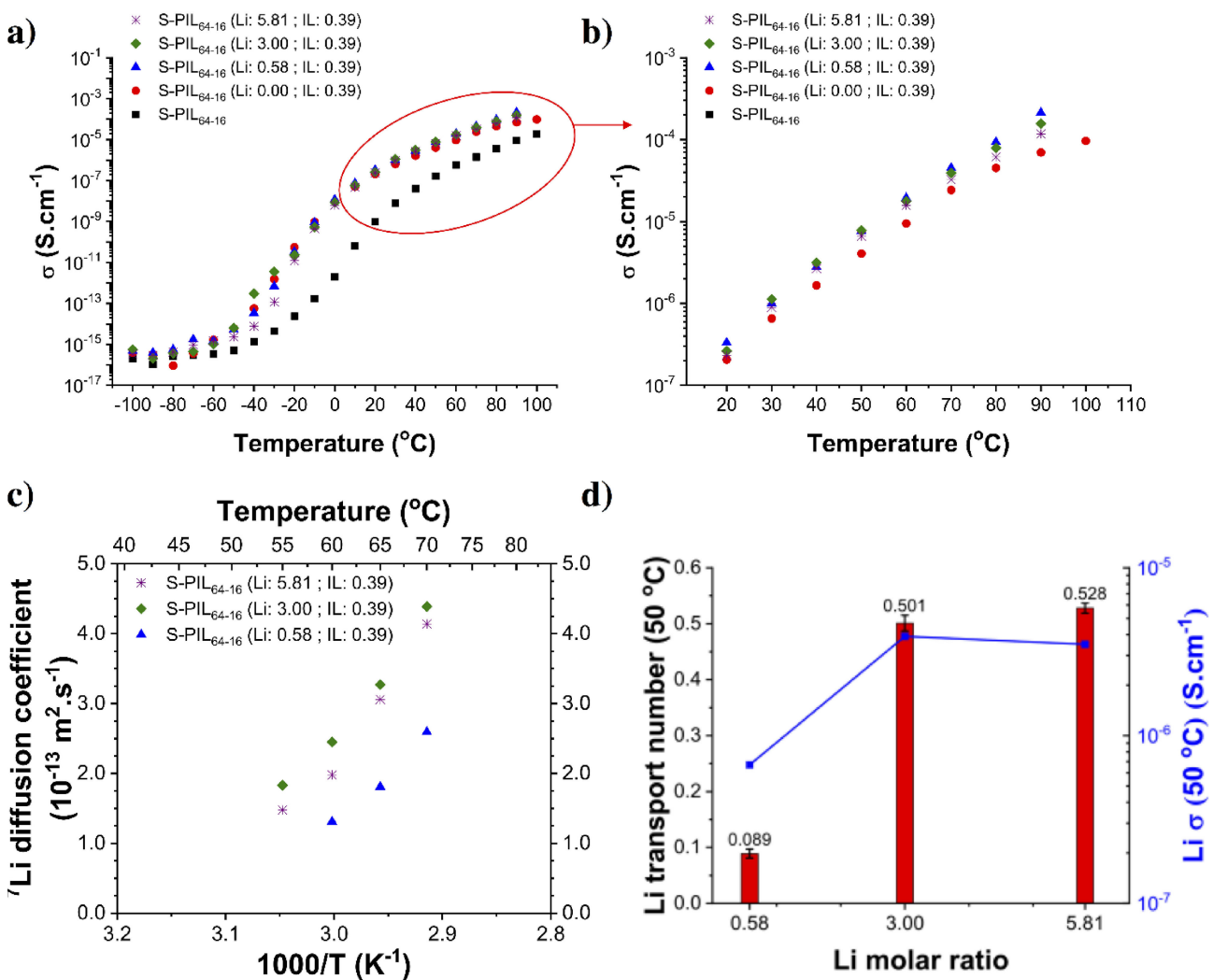


Figure 2. Ionic conductivity (a, b: zoom plot of a) and lithium diffusion coefficient (c) of the S-PIL₆₄₋₁₆ electrolytes as a function of temperature. Lithium transport number and corresponding Li-ion conductivity of the S-PIL₆₄₋₁₆ electrolytes at 50 °C (d)

decreasing ionic conductivity for an Li molar ratio ≥ 3.00 is possibly due to the formation of multidendate FSI/TFSI anion-Li-coordination due to the high content of lithium salt, resulting in significant aggregation.^[9,45] Indeed, a decrease of anion (FSI and TFSI) to Li⁺ molar ratio (from 3.4 to 1.2) is observed when a Li molar ratio of 0.58 and 5.81 are used, respectively.

The formation of Li anion complexes with FSI/TFSI ligands is thus required in order to satisfy the lithium coordination environment (coordination number for Li⁺ is typically ranging between 3 and 5).^[9,45]

While EIS measurements are able to provide detailed insights into the overall ion dynamics of the S-PIL₆₄₋₁₆ electrolytes upon IL and LiFSI addition, the inability to distinguish the contribution of individual ionic species is the main limitation of this technique. For this reason, ⁷Li pulsed field gradient (PFG) diffusion NMR and lithium transport number (t^{Li^+}) measurements were carried out in order to quantify the lithium dynamics of these systems and the results are given in Figure 2c and d. Figure 2c shows the lithium diffusion coefficient as a function of temperature for the S-PIL₆₄₋₁₆ electrolytes

at a fixed IL molar ratio of 0.39 and with increasing Li molar ratio. Over the temperature range studied, a significant increase in the lithium diffusion coefficient is observed when Li molar ratio is increased from 0.58 to 3.00. As an example, a lithium diffusion coefficient of 1.3×10^{-13} m²·s⁻¹ and 2.5×10^{-13} m²·s⁻¹ is measured at 60 °C for a Li molar ratio of 0.58 and 3.00, respectively. This increase in lithium diffusion coefficient, along with the ionic conductivity data in Figure 2a, which showed no improvements when Li molar ratio is increased from 0.58 to 3.00, suggests that the long-range charge migration (detected by EIS) occurs with a mechanism different from that of simple exchange of charge revealed by NMR. This is in perfect accordance with other studies which demonstrated that in presence of mesoscale heterogeneities the long-range charge migration occurs owing to the exchange/hopping of charge between delocalization bodies.^[9,46,47] A further increase in Li molar ratio results in a slight decrease in lithium ion diffusion coefficient over the temperature range studied, although this is less pronounced for temperatures above 65 °C. This decrease in lithium diffusion coefficient coincides with the slight decrease

in ionic conductivity observed when the Li molar ratio is increased from 3.00 to 5.81. This suggests that the overall ion mobility decreases slightly, while still remaining higher than for lower Li molar ratio.

Additionally, the lithium transport number (t^{Li^+}) of the S-PIL₆₄₋₁₆ electrolytes was also measured at 50 °C using the Bruce-Vincent-Evans technique. From these values and the overall ion conductivity, the Li-ion conductivity was extrapolated (Li-ion σ (50 °C) = σ_{EIS} (50 °C) * t^{Li^+}) and the results presented in Figure 2d. A t^{Li^+} of 0.09 is obtained for the S-PIL₆₄₋₁₆ (Li: 0.58; IL: 0.39) electrolyte at 50 °C, which is quite a low value when compared to other lithium-based electrolyte systems.^[9,31] This low t^{Li^+} value coupled with the moderate ionic conductivity of S-PIL₆₄₋₁₆ (Li: 0.58; IL: 0.39) electrolyte results in a poor Li-ion conductivity of $6.7 \cdot 10^{-7} \text{ Scm}^{-1}$ at 50 °C. Increasing the Li molar ratio from 0.58 to 3.00 results in a dramatic increase of the t^{Li^+} to 0.50, which is one of the highest t^{Li^+} reported to date for a polymeric electrolyte (excluding single-ion conducting polymers).^[34-37] As an example, a t^{Li^+} of only 0.1–0.2 is generally reported for poly(ethylene oxide)-based polymer electrolytes, which is commonly considered as the benchmark SPE system.^[31,34,38] The increase in t^{Li^+} observed for the S-PIL₆₄₋₁₆ (Li: 3.00; IL: 0.39) suggests that the transport mechanism in these systems has changed, favouring lithium ion mobility. Such an increase

results in a Li-ion conductivity of $3.9 \cdot 10^{-6} \text{ Scm}^{-1}$ at 50 °C. Further increase of the Li molar ratio from 3.00 to 5.81 only results in a slight change of the t^{Li^+} to 0.53, which overall corresponds to a slight decrease of Li-ion conductivity to $3.5 \cdot 10^{-6} \text{ Scm}^{-1}$ at 50 °C. These results are remarkably consistent with the ⁷Li NMR diffusion results.

Figure 3 shows the galvanostatic cycling of lithium symmetrical (Li|Li) cells at 50 °C, using various current densities ranging from 0.02 mA cm⁻² to 0.2 mA cm⁻², and a polarization period of 20 minutes. As can be seen in Figure 3a, a high but stable cell polarization of ca. 0.17 V is observed at a relatively low current density (0.02 mA cm⁻²), when using the S-PIL₆₄₋₁₆ (Li: 0.58; IL: 0.39) electrolyte. Increasing the current density to 0.05 mA cm⁻² results in a large polarization and unstable profile, reaching the voltage cut-off of 5 V after only 9.6 minutes of charge. Increasing the Li molar ratio to 3.00 (Li: 3.00; IL: 0.39) results in a significant enhancement of the cycling performance with stable cycling observed up to a current density of 0.20 mA cm⁻². The polarization results obtained for the S-PIL₆₄₋₁₆ (Li: 3.00; IL: 0.39) system clearly illustrates the importance of high Li-ion conductivity vs. high overall ionic conductivity (i.e. from all ionic species), and how such Li mobility can be achieved by the use of highly concentrated electrolytes.

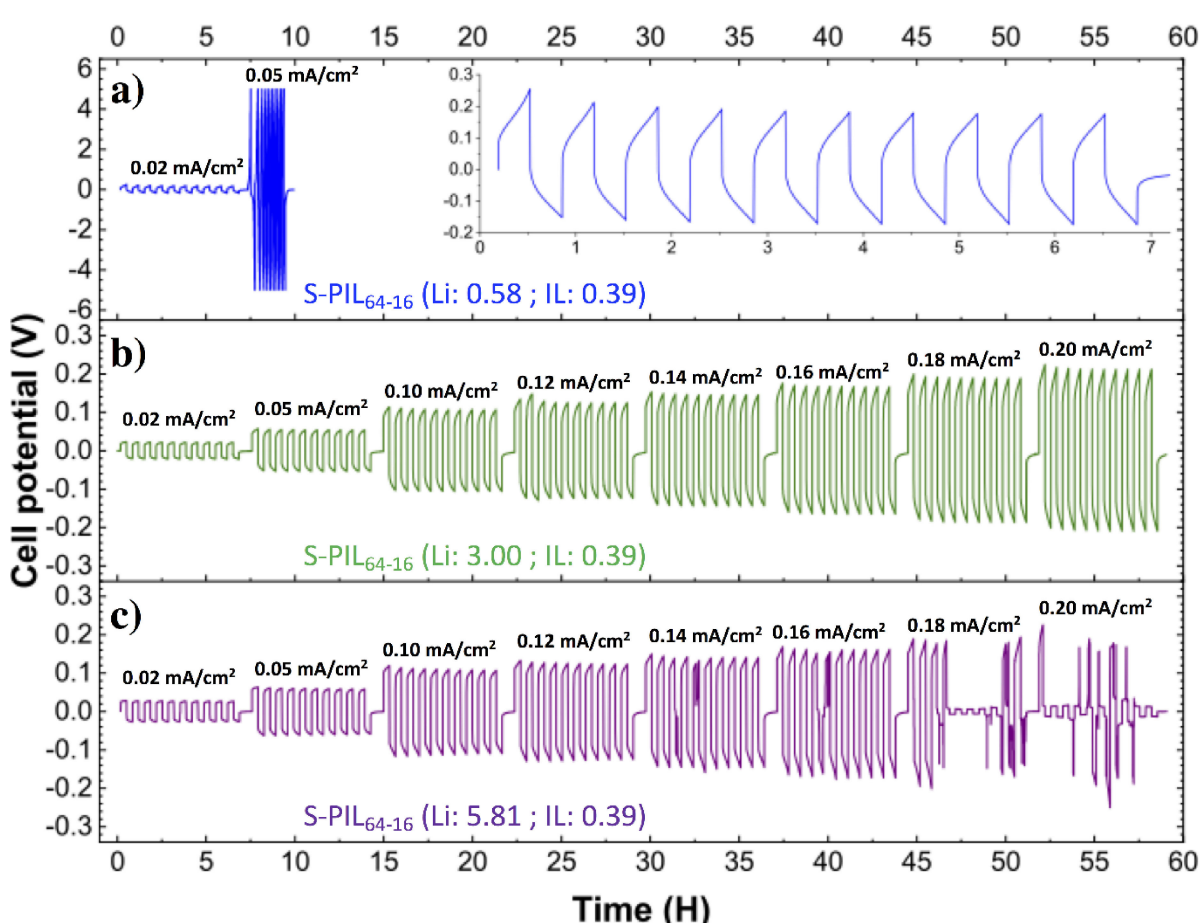


Figure 3. Galvanostatic cycling of lithium symmetrical cells at 50 °C using S-PIL₆₄₋₁₆ electrolytes: impact of lithium salt concentration. A polarization period of 20 mins were used for all current densities, corresponding to an areal capacity of 0.03 mAh cm⁻² when a current density of 0.1 mA cm⁻² is used.

Stable polarizations are also observed for a current density up to 0.12 mA cm^{-2} for the S-PIL₆₄₋₁₆ (**Li**: 5.81; **IL**: 0.39) system, although behaviour indicative of micro-short circuiting is observed when higher current densities are used. The initiation of micro-short circuiting can be attributed to the softening of the material when the **Li** molar ratio is increased from 3.00 to 5.81. The galvanostatic cycling of thicker S-PIL₆₄₋₁₆ (**Li**: 5.81; **IL**: 0.39) membranes (*ca.* 120 μm vs. 350 μm) results in a stable polarization of *ca.* 0.22 V at 0.20 mA cm^{-2} , supporting the hypothesis that mechanical properties (i.e. ability to mechanically resist dendrite growth) has a greater influence over the ability to prevent micro-short circuiting than does the ionic conductivity. It is also important to note that the use of such high lithium ion concentration with a PIL homopolymer (poly(diallyldimethyl-ammonium)bis(trifluoromethanesulfonyl)imide, PDADMA TFSI) was also attempted for comparison and it was found that a soft gel material with little mechanical integrity is produced (see supporting information). This further highlights the superior mechanical properties of PIL block copolymer electrolytes, especially in relation to dendrite suppression.

To better quantify the mechanical properties of the S-PIL₆₄₋₁₆ electrolyte, the storage modulus (G') and the loss modulus (G'') were also determined for S-PIL₆₄₋₁₆ (**Li**: 3.00; **IL**: 0.39) system in a shear mode at both 30 °C and 50 °C. Results are summarised in Table 1. At 30 °C, the S-PIL₆₄₋₁₆ (**Li**: 3.00; **IL**: 0.39) electrolyte

Table 1. Summary of the mechanical properties of the S-PIL ₆₄₋₁₆ (Li : 3.00; IL : 0.39) electrolyte in a shear mode at both 30 °C and 50 °C.		
Temperature	Storage Modulus (G') [MPa] ^[a,b]	Loss Modulus (G'') [MPa] ^[a,b]
30 °C	3.1	0.7
50 °C	1.4	1.2

[a] Errors are estimated at $\pm 20\%$ [b] Measured at 1 Hz.

exhibits a storage modulus and a Loss modulus of 3.1 MPa and 0.7 MPa, respectively. Increasing temperature to 50 °C results in a slight decrease of the storage modulus to 1.4 MPa. Under this experimental condition, the storage modulus is always higher than that of the loss modulus for both temperatures, suggesting a solid-like behaviour.^[11]

Before assessing the cycling performance of the S-PIL₆₄₋₁₆ electrolyte in a full cell, their electrochemical stability towards oxidation needs to be assessed, using lithium-metal|S-PIL₆₄₋₁₆ electrolyte|stainless steel cells. Figure 4 shows the linear sweep voltammograms (LSV) of the S-PIL₆₄₋₁₆ electrolyte at 50 °C. The S-PIL₆₄₋₁₆ (**Li**: 3.00; **IL**: 0.39) electrolyte shows an oxidation potential of about 4.5 V vs. Li⁺/Li, which is slightly higher than that of the conventional PEO based electrolyte (*ca.* 3.8 V vs. Li⁺/Li).^[46] Interestingly, increasing **Li** molar ratio to 5.81 results in a decrease of the current density of the minor oxidation process at around 4.5 V vs. Li⁺/Li, from 0.27 to 0.17 $\mu\text{A cm}^{-2}$. Additionally, the second oxidation process at around 5.4 V vs. Li⁺/Li for S-PIL₆₄₋₁₆ (**Li**: 5.81; **IL**: 0.39) is not as pronounced as for the S-PIL₆₄₋₁₆ (**Li**: 3.00; **IL**: 0.39) system. It also worth pointing out that the current densities observed for S-PIL₆₄₋₁₆ electrolyte are

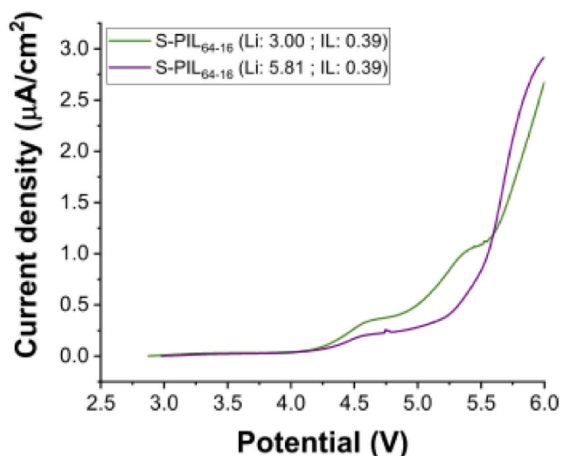


Figure 4. Linear sweeping voltammetry profiles of the lithium-metal|S-PIL₆₄₋₁₆ electrolyte|stainless steel (SS) cells using either the S-PIL₆₄₋₁₆ (**Li**: 3.00; **IL**: 0.39) or S-PIL₆₄₋₁₆ (**Li**: 5.81; **IL**: 0.39) electrolytes at 50 °C.

quite low, with a current density not exceeding 0.5 $\mu\text{A cm}^{-2}$ up to a voltage of 5.2 V vs. Li⁺/Li for the S-PIL₆₄₋₁₆ (**Li**: 5.81; **IL**: 0.39) system, potentially allowing them to be used in conjunction with high voltage cathode such as lithium cobalt oxide (LCO) or lithium nickel manganese cobalt oxide (NMC).

Finally, the cycling performance of the S-PIL₆₄₋₁₆ (**Li**: 5.81; **IL**: 0.39) electrolyte has also been tested in a rechargeable lithium-metal battery (LMB) at 50 °C, using a lithium iron phosphate (LiFePO₄) based cathode. Figure 5 shows the charge/discharge profile

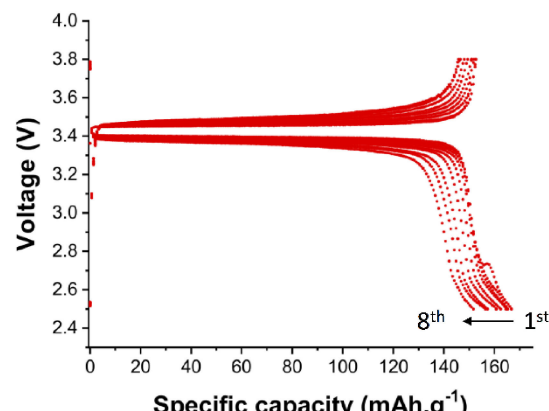


Figure 5. Charge/discharge profile of a lithium-metal|S-PIL₆₄₋₁₆ (**Li**: 5.81; **IL**: 0.39) electrolyte|LFP cell with an areal capacity of 1.8 mAh cm^{-2} at a C-rates of C/20.

profile of a Li|LiFePO₄ cell with an areal capacity of 1.8 mAh cm^{-2} , at a C-rate of C/20. A discharge capacity of 167 mAh g^{-1} is achieved for the first cycle, which is almost equal to the theoretical capacity of LiFePO₄ (170 mAh g^{-1}).^[48] A slight capacity fade is observed in the following cycles, resulting in a 6.3% capacity loss after 8 cycles. The discharge voltage profile in Figure 5 shows a change of slope below 2.7 V vs. Li⁺/Li, which could likely indicate that some irreversible

reactions are occurring and could contribute to the capacity fading.^[47] Nevertheless, the capacities obtained during these first cycles are still very promising and confirms the potential of these materials as polymer electrolyte for LMBs. Further optimization of the polymer electrolyte and the cathode composition is currently under investigation in order to improve the long-term cycling stability of these materials.

In conclusion, a ternary polymer electrolyte system has been developed using a novel PIL block copolymer as a polymer host for mechanical reinforcement. The phase behaviour and ion transport properties of S-PIL₆₄₋₁₆ electrolytes were characterized upon IL and lithium salt addition. S-PIL₆₄₋₁₆ electrolytes with high Li-ion conductivity were formulated by limiting the overall anion to Li⁺ molar ratio to 1.5 and below, corresponding to a Li molar ratio of 3.00 and above. These S-PIL₆₄₋₁₆ (Li: ≥ 3.00; IL: 0.39) electrolytes exhibit high compatibility with lithium-metal electrodes and stable cycling performances of up to 0.20 mA cm⁻² in a lithium symmetrical cell. Finally, a rechargeable all solid-state lithium-metal battery was developed using a solid-state lithium iron phosphate (LiFePO₄) based cathode with areal capacity of 1.8 mAh cm⁻² and the S-PIL₆₄₋₁₆ (Li: 5.81; IL: 0.39) as electrolyte. Near theoretical discharge capacity of 167 mAh g⁻¹ was achieved for the first cycle, confirming the potential of these materials as polymer electrolyte for LMBs.

Experimental Section

Polymer Electrolyte Preparation

S-PIL₆₄₋₁₆ electrolyte was prepared by solvent casting. A 10 wt.% solution was prepared by dissolving the appropriate amount of S-PIL₆₄₋₁₆ polymer, LiFSI and/or C₃mpyrFSI in tetrahydrofuran (THF). 1.8 mL of the S-PIL_{n-m} electrolyte solution was casted onto an in-house designed Teflon mold (60 L × 20 W × 0.5 D, mm) inside a glovebox and the solvent was allowed to evaporate for 24 h. The S-PIL₆₄₋₁₆ electrolyte film was then dried under high vacuum at 80 °C for 24 h, resulting in 100–120 μm thick polymer film.

Differential Scanning Calorimetry (DSC)

Differential Scanning Calorimetry measurements were performed on a Mettler Toledo DSC 1 Star^e instrument. DSC instrument was calibrated using cyclohexane. The samples were accurately weighed into standard sealed aluminium pans. The samples were heated from 178.15 K to 393.15 K and then cooled down from 393.15 K to 178.15 K at rate of 10 K min⁻¹. Isothermal steps of 10 and 5 min were added at 178.15 K and 393.15 K, respectively. This cycle was repeated three times.

Small-Angle X-Ray Scattering (SAXS)

Synchrotron SAXS measurements were performed at the Australian Synchrotron on the SAXS/WAXS beamline. An in-vacuum undulator (22 mm period, 3 m length, K_{max} = 1.56) with a beam energy of 16 keV and a 7 m camera length were used, allowing a detection range for a momentum transfer of 0.003 Å⁻¹ < q < 0.171–0.215 Å⁻¹. The two-dimensional SAXS patterns were recorded with a 1 M Pilatus detector with 981 × 1043 pixel resolution.

Dynamic Mechanical Analysis (DMA)

Dynamic mechanical analysis measurements were performed on a PerkinElmer DMA 8000 instrument, in a shear mode configuration. Circular disk specimens (8 mm in diameter and 200–250 μm thick) were prepared and measured over a frequency range of 0.1 to 100 Hz at a fixed strain amplitude of 0.5%. Measurements were performed at both 30 °C and 50 °C.

Cathode Preparation

A slurry of LiFePO₄ based cathode was prepared by mixing LiFePO₄ powder (ALEEES), Super C65 (Timcal) and a conducting polymer (60:10:30 wt.%) in NMP using a Flacktek Speedmixer (DAC 150) at 3000 rpm for 5 minutes. The prepared slurry was cast onto an aluminium current collector using a doctor blade casting method (200 μm, RK automatic film applicator) and the solvent was allowed to evaporate for 24 h. The cathode electrode was then further dried under high vacuum at 50 °C for 24 h, resulting in an LiFePO₄ loading of 10.7 mg cm⁻².

Electrochemical Characterization

The ionic conductivity of S-PIL₆₄₋₁₆ electrolyte was measured by electrochemical impedance spectroscopy (EIS) in the frequency range from 10⁻² to 10⁷ Hz, using Novocontrol Alpha-A analyser over a temperature range, from 173.15 K to 373.15 K. The temperature was controlled using a customized cryostat operating with a heating N2 gas jet and a liquid nitrogen-based cooling system. The S-PIL₆₄₋₁₆ electrolyte was sandwiched between two circular platinum electrodes (ca. 13 mm in diameter) and sealed in a cylindrical Teflon cell with stainless steel case. The distance between the two electrodes was controlled using a separator consisting of two optical fibres with a diameter of 126 μm. The hermetic cell was assembled inside an argon glovebox. Li|Li and Li|LiFePO₄ cells (CR2032) were assembled in an argon glovebox, using a 6 mm diameter lithium electrode (Gelon, 100 μm thick). All Li|Li and Li|LiFePO₄ cells were stored at 50 °C for 24 h, straight after assembly, prior to any galvanostatic cycling being carried out. Galvanostatic cycling for both Li|Li and Li|LiFePO₄ cells was performed using a multi-channel potentiostat VMP3 (Bio-Logic) and a battery tester (Neware), respectively. The evolution of both electrolyte and SEI resistance ($R_{\text{Cell}} = R_{\text{Electrolyte}} + R_{\text{SEI}}$) of Li|Li cells during a resting period of 24 h at 50 °C was monitored by EIS using a multi-channel potentiostat VMP3 (Bio-Logic). The AC impedance spectra were recorded in a frequency range from 10⁻¹ to 10⁶ Hz. The t^{L+} of the S-PIL₆₄₋₁₆ electrolyte at 50 °C was measured in accordance with the method described by Evans et. al. using Li|Li cells.^[48–50] The Linear sweep voltammogram (LSV) were performed at 50 °C, in a two-electrode coin cell configuration, using stainless steel and lithium-metal electrodes as working electrode and both counter and reference electrodes, respectively. LSV measurement were carried out from open circuit potential to 6.0 V vs. Li⁺/Li at a fixed scan rate of 0.5 mV s⁻¹.

Pulsed Field Gradient (PFG) Diffusion NMR

⁷Li PFG NMR diffusion measurements were performed on a Bruker Avance 300 MHz wide-bore NMR spectrometer using the pulsed field gradient stimulated echo (PGSTE) sequence. A maximum gradient strength of 2400 G/cm was used. The repetition time were kept around 6–10 s depending on the temperature. In some cases, the repetition times were also increased in order to reduce the duty circle of the gradient system. The diffusion time Δ is was specified between 200 to 1100 ms to maintain the square root of

the mean square displacement $R = \sqrt{6D\Delta}$ in the scale of 0.2–0.7 μm. The diffusion coefficients were calculated using the Stejskal-Tanner equation:

$$\frac{S}{S(0)} = \exp[-\gamma^2 D \delta^2 \left(\Delta - \frac{1}{3} \delta \right) g^2]$$

Where γ is the gyromagnetic ratio, D is the diffusion coefficients (m²/s), δ is the gradient pulse duration (s), Δ is the diffusion duration (s) and g is the gradient strength (G/m). The ratio $S/S(0)$ denotes for the signal attenuation, in which, S is the signal intensity observed at g gradient strength while $S(0)$ is the signal intensity at zero gradient strength.

Acknowledgements

This work was supported by the Australian Research council (ARC) through the Australian Laureate Fellowships FL110100013 (MF), the office of the DVCR, Deakin University and CSIRO. The authors acknowledge funding for beamtime M11752 on the SAXS/WAXS beamline at the Australian Synchrotron, Victoria, Australia and the support from beamline scientist, Dr Adrian Hawley.

Conflict of Interest

The authors declare no conflict of interest.

Keywords: high lithium transport number • ionic liquids • polymerized ionic liquid block copolymer • lithium-metal batteries • solid polymer electrolytes

- [1] R. Bouchet, S. Maria, R. Meziane, A. Aboulaich, L. Lienafa, J. P. Bonnet, T. N. T. Phan, D. Bertin, D. Gigmes, D. Devaux, R. Denoyel, M. Armand, *Nat. Mater.* **2013**, *12*, 452–457.
- [2] B. Dunn, H. Kamath, J.-M. Tarascon, *Science* **2011**, *334*, 928–935.
- [3] P. Adelhelm, P. Hartmann, C. L. Bender, M. Busche, C. Eufinger, J. Janek, *Beilstein J. Nanotechnol.* **2015**, *6*, 1016–1055.
- [4] J. S. Lee, S. T. Kim, R. Cao, N. S. Choi, M. Liu, K. T. Lee, J. Cho, *Adv. Energy Mater.* **2011**, *1*, 34–50.
- [5] P. C. Howlett, N. Brack, A. F. Hollenkamp, M. Forsyth, D. R. MacFarlane, *J. Electrochem. Soc.* **2006**, *153*, A595–A606.
- [6] D. R. MacFarlane, M. Forsyth, P. C. Howlett, M. Kar, S. Passerini, J. M. Pringle, H. Ohno, M. Watanabe, F. Yan, W. Zheng, S. Zhang, J. Zhang, *Nat. Rev. Mater.* **2016**, *1*, 1–15.
- [7] I. Osada, H. De Vries, B. Scrosati, S. Passerini, *Angew. Chem. Int. Ed.* **2016**, *55*, 500–513.
- [8] X. Ji, L. F. Nazar, *J. Mater. Chem.* **2010**, *20*, 9821–9826.
- [9] M. Forsyth, G. M. A. Girard, A. Basile, M. Hilder, D. R. MacFarlane, F. Chen, P. C. Howlett, *Electrochim. Acta* **2016**, *220*, 609–617.
- [10] C. Monroe, J. Newman, *J. Electrochem. Soc.* **2005**, *152*, A396–A404.
- [11] G. M. Stone, S. A. Mullin, A. A. Teran, D. T. Hallinan, A. M. Minor, A. Hexemer, N. P. Balsara, *J. Electrochem. Soc.* **2012**, *159*, A222–A227.
- [12] V. Di Noto, S. Lavina, G. A. Giffin, E. Negro, B. Scrosati, *Electrochim. Acta* **2011**, *57*, 4–13.
- [13] T. M. Bennett, K. S. Jack, K. J. Thurecht, I. Blakey, *Macromolecules* **2016**, *49*, 205–214.
- [14] J. M. Virgili, A. Hexemer, J. A. Pople, N. P. Balsara, R. A. Segalman, *Macromolecules* **2009**, *42*, 4604–4613.
- [15] A. A. Rojas, S. Inceoglu, N. G. Mackay, J. L. Thelen, D. Devaux, G. M. Stone, N. P. Balsara, *Macromolecules* **2015**, *48*, 6589–6595.
- [16] A. L. Pont, R. Marcilla, I. De Meataz, H. Grande, D. Mecerreyes, *J. Power Sources* **2009**, *188*, 558–563.
- [17] X. Wang, H. Zhu, G. M. A. Girard, R. Yunis, D. R. MacFarlane, D. Mecerreyes, A. J. Bhattacharya, P. C. Howlett, M. Forsyth, *J. Mater. Chem. A* **2017**, *5*, 23844–23852.
- [18] N. Boaretto, C. Joost, M. Seyfried, K. Vezzù, V. Di Noto, *J. Power Sources* **2016**, *325*, 427–437.
- [19] V. Di Noto, M. Vittadello, K. Yoshida, S. Lavina, E. Negro, T. Furukawa, *Electrochim. Acta* **2011**, *57*, 192–200.
- [20] M. Jeyapandian, S. Lavina, S. Thayumanasundaram, H. Ohno, E. Negro, V. Di Noto, *J. Power Sources* **2010**, *195*, 341–353.
- [21] K. (Kelvin) Fu, Y. Gong, J. Dai, A. Gong, X. Han, Y. Yao, C. Wang, Y. Wang, Y. Chen, C. Yan, Y. Li, E. D. Wachsman, L. Hu, *Proc. Natl. Acad. Sci.* **2016**, *113*, 7094–7099.
- [22] H. Kim, Y. Shul, H. Han, *2006*, *158*, 137–142.
- [23] D. R. Sadoway, *J. Power Sources* **2004**, *129*, 1–3.
- [24] P. E. Trapa, Y.-Y. Won, S. C. Mui, E. A. Olivetti, B. Huang, D. R. Sadoway, A. M. Mayes, S. Dallek, *J. Electrochem. Soc.* **2005**, *152*, A1–A5.
- [25] A. Panday, S. Mullin, E. D. Gomez, N. Wanakule, V. L. Chen, A. Hexemer, J. Pople, N. P. Balsara, *Macromolecules* **2009**, *42*, 4632–4637.
- [26] M. Singh, O. Odusanya, G. M. Wilmes, H. B. Eitouni, E. D. Gomez, A. J. Patel, V. L. Chen, M. J. Park, P. Fragouli, H. Iatrou, N. Hadjichristidis, D. Cookson, N. P. Balsara, *Macromolecules* **2007**, *40*, 4578–4585.
- [27] V. Di Noto, E. Negro, S. Lavina, M. Vittadello, *Polym. Electrolytes* **2010**, *219*, 219–277.
- [28] M. A. Ratner, D. F. Shriver, *Chem. Rev.* **1988**, *109*–124.
- [29] M. Armand, *Solid State Ionics* **1983**, *9 & 10*, 745–754; *10*, 745–754.
- [30] K. Kimura, M. Yajima, Y. Tominaga, *Electrochim. Commun.* **2016**, *66*, 46–48.
- [31] Y. Tominaga, K. Yamazaki, *Chem. Commun.* **2014**, *50*, 4448–4450.
- [32] V. Di Noto, D. Longo, V. Münchow, *J. Phys. Chem. B* **1999**, *103*, 2636–2646.
- [33] V. Di Noto, M. Vittadello, S. Lavina, M. Fauri, S. Biscazzo, *J. Phys. Chem. B* **2001**, *105*, 4584–4595.
- [34] S. H. Chung, Y. Wang, L. Persi, F. Croce, S. G. Greenbaum, B. Scrosati, E. Plichta, *J. Power Sources* **2001**, *97–98*, 644–648.
- [35] B. Scrosati, F. Croce, L. Persi, *J. Electrochem. Soc.* **2000**, *147*, 1718–1721.
- [36] J. Mindemark, B. Sun, E. Törmä, D. Brandell, *J. Power Sources* **2015**, *298*, 166–170.
- [37] L. Porcarelli, C. Gerbaldi, F. Bella, J. R. Nair, *Sci. Rep.* **2016**, *6*, 1–14.
- [38] X. Judez, M. Piszcza, E. Coya, C. Li, I. Aldalur, U. Oteo, Y. Zhang, W. Zhang, L. M. Rodriguez-Martinez, H. Zhang, M. Armand, *Solid State Ionics* **2017**, *318*, 95–101.
- [39] A. M. Stephan, *Eur. Polym. J.* **2006**, *42*, 21–42.
- [40] G. B. Appetecchi, G. T. Kim, M. Montanino, M. Carewska, R. Marcilla, D. Mecerreyes, I. De Meataz, *J. Power Sources* **2010**, *195*, 3668–3675.
- [41] A. S. Shaplov, R. Marcilla, D. Mecerreyes, *Electrochim. Acta* **2015**, *175*, 18–34.
- [42] J. Yuan, D. Mecerreyes, M. Antonietti, *Prog. Polym. Sci.* **2013**, *38*, 1009–1036.
- [43] D. Mecerreyes, *Prog. Polym. Sci.* **2011**, *36*, 1629–1648.
- [44] L. Gwee, J.-H. Choi, K. I. Winey, Y. A. Elabd, *Polymer (Guildf.)* **2010**, *51*, 5516–5524.
- [45] F. Chen, M. Forsyth, *Phys. Chem. Chem. Phys.* **2016**, *18*, 19336–19344.
- [46] I. Aldalur, M. Martinez-Ibañez, M. Piszcza, H. Zhang, M. Armand, *Batter. Supercaps* **2018**, 149–159.
- [47] R. Younesi, G. M. Veith, P. Johansson, K. Edström, T. Vegge, *Energy Environ. Sci.* **2015**, *8*, 1905–1922.
- [48] J. Evans, C. A. Vincent, P. G. Bruce, *Polymer* **1987**, *28*, 2324–2328.
- [49] P. G. Bruce, C. A. Vincent, *J. Chem. Soc. Faraday* **1993**, *89*, 3187–3203.
- [50] K. M. Abraham, Z. Jiang, B. Carroll, *Chem. Mater.* **1997**, *9*, 1978–1988.

Manuscript received: October 11, 2018

Revised manuscript received: November 19, 2018

Version of record online: December 13, 2018